

A.A. Ivanov^{1,2,3}, A.R. Krylov¹, A.G. Molokanov¹, A.Yu. Bushmanov², A.S. Samoylov²,
E.E. Pavlik¹, G.V. Mytsin¹, S.V. Shvidky¹, G.N. Timoshenko^{1,4}

MODELING OF LABORATORY ANIMALS EXPOSURE CONDITIONS BEHIND LOCAL CONCRETE SHIELDING BOMBARDED BY 650-MEV PROTONS

¹ Joint Institute for Nuclear Research, Dubna, Russia;

² A.I. Burnasyan Federal Medical Biophysical Center, Moscow, Russia;

³ Institute of Biomedical Problems of RAS, Moscow, Russia;

⁴ Dubna State University, Dubna, Russia

Контактное лицо: G.N. Timoshenko, tim@jinr.ru

ABSTRACT

Purpose: To estimate the radiation fields formed after the passage of high-energy protons through the concrete protection for subsequent radiobiological experiments on animals on this model.

Material and methods: The results of the calculation of the secondary characteristics of a field of mixed radiation behind the local concrete with thickness 20, 40, and 80 cm, bombarded by a proton beam of 650 MeV at the JINR Phasotron and experimental estimation of the values of the absorbed dose phantoms of mice irradiated for protection during radiobiological experiments.

The calculation was performed by the Monte Carlo method according to the MCNPX program for secondary protons, neutrons, π -mesons, and gamma rays. To verify the adequacy of calculations was performed the comparison of calculated and measured in the experiment spatial distribution of activation threshold detectors for aluminum protection, as well as a comparison of the calculated values of absorbed dose for radiation protection with the results of absorbed dose measurements with a diamond detector.

Results: The calculations made it possible to obtain the characteristics of the fields of mixed secondary radiation behind local concrete shields of different thickness irradiated with protons with an energy of 650 MeV and to estimate the values of absorbed doses in the irradiation sites of mice in the radiobiological experiment. The reliability of the calculations was confirmed by experimental verification of the activation of aluminum threshold detectors behind a 20 cm thick protection, as well as direct measurements using a diamond detector.

Conclusion: The calculated assessment of radiation fields formed after protons pass through the concrete protection and its comparison with the results of radiation dose measurements for the subsequent radiobiological experiment on animals on this model in the interests of designing protective structures on the Moon and other space bodies, as well as biological defenses on charged-particles accelerators.

Key words: *proton beam, secondary radiation field, absorbed dose, radiation transport in a matter, concrete shielding, radiobiological experiment, regolith*

For citation: Ivanov AA, Krylov AR, Molokanov AG, Bushmanov AYu, Samoylov AS, Pavlik EE, Mytsin GV, Shvidky SV, Timoshenko GN. Modeling of Laboratory Animals Exposure Conditions behind Local Concrete Shielding Bombarded by 650-MeV Protons. Medical Radiology and Radiation Safety. 2020;65(5):77-86.

DOI: 10.12737/1024-6177-2020-65-5-77-86

Introduction

During the operation of research and medical accelerators of high-energy charged particles, as well as during space flights, a person may be exposed to radiation fields of different nature. There are particles from cosmic radiation, which astronauts can be irradiated when they go into outer space or stay on the surface of the Moon or Mars, or, in cases of medical exposure of patients, accelerated charged particles. The secondary radiation fields behind the accelerator shielding are similar to the radiation fields arising from the interaction of space radiation with the shell and elements of the spacecraft. In addition to the above, there is irradiation from induced radioactivity. All these sources of radiation hazard must be taken into account, in particular, when designing shelters on the Moon and Mars. Most likely, for the construction of a protective building on the Moon or Mars, the lunar and Martian regolith will be used, which, in many respects, coincides in chemical composition with concrete which uses for radiation protection of nuclear physics facilities [1, 2]. In principle, the energy of galactic space particles can spread to huge value, but the maximum in the proton spectrum is near the energy of

the accelerated protons of the JINR Laboratory of Nuclear Problem phasotron.

The adequate calculation of radiation fields behind radiation shields can be carried out using a universal code for the transport of radiation in the matter by the Monte Carlo method [3]. These calculations should be supported by experimental testing, and also, in our opinion [4], by a radiobiological experiment on animals, since in this case, we obtain a direct integral assessment of the hazard of radiation exposure. All of the above made it possible to formulate the goal of this work as a calculated phantom estimate of the radiation fields formed after the passage of protons through a concrete shield and its comparison with the results of experimental testing for subsequent radiobiological experiments on animals on this model.

Material and methods

Before a radiobiological experiment on irradiation of mice with secondary radiation emitted from a local concrete shield of various thickness, irradiated by a proton beam with an energy of 650 MeV at the phasotron of the Laboratory of Nuclear Problems of the Joint Institute for Nuclear Research, mathematical modeling

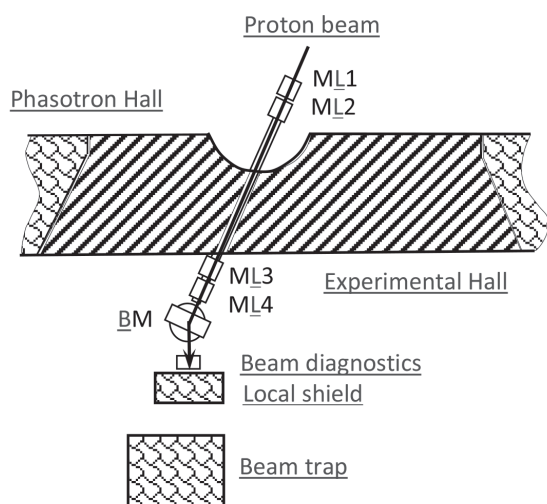


Fig. 1. Geometry of the experimental stand at the phasotron
ML — magnetic lenses, BM — bending magnet

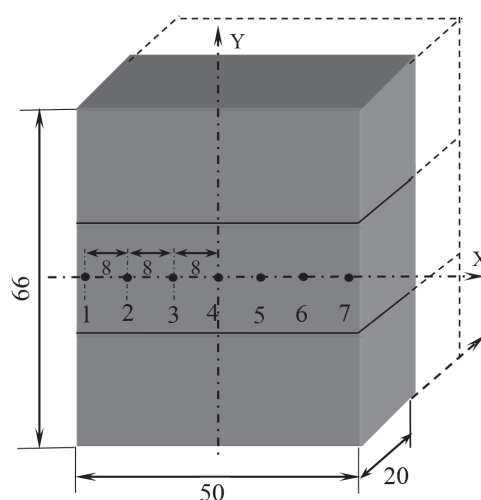


Fig. 2. Frontal projection of local shield

of the experiment was carried out using a universal code for the transport of radiation in the matter by the Monte Carlo method MCNPX ver. 6.2 [3] and experimental verification of the calculation results were carried out as well.

A stand for irradiation of animals was located in the experimental hall of the phasotron, separated from the accelerator by a massive shield. A beam of 650 MeV protons extracted from the phasotron, was transported with a magneto-optical channel consisting of two doublets of quadrupole lenses through a collimator in a shield to the experimental hall. In the hall, the proton beam was focused using a quadrupole lens doublet and a bending magnet and directed to an experimental stand consisting of a local shield and a beam diagnostics system (Fig. 1). Irradiation of animals is planned directly behind the local shields, in horizontally located cages — cells made of radiation-permeable material.

The local shield was mounted from ordinary concrete blocks 50 cm long, 20 cm wide, and 22 cm high with a density of 2.15 g/cm^3 . The total thickness of the shield along the beam was varied in the experiment from 20 to 80 cm. Behind the stand, at a distance of 1.5 m from it, there was a massive concrete beam trap, in which secondary radiation from the stand was absorbed. The horizontal and vertical profiles of the primary proton beam at the entrance to the local shield were measured using a multiwire ionization chamber. The intensity of the beam incident on the shield was measured with a plane-parallel wide-aperture air ionization chamber. The energy of the protons of the beam in the place of their entrance to the shield was estimated at 650 MeV.

Calculation of secondary radiation fields behind local shields

In the cascade of internuclear interactions when calculating the radiation fields behind the local shields and in the calculated doses received by laboratory animals were included protons, neutrons, π^+ and π^- mesons,

deuterons, ^3He and ^4He nuclei. The development of an electron-photon shower and the production of photoneutrons was also taken into account.

The beam of protons incident under the normal to the center of the local shield was accepted to be monoenergetic in the calculations. The spatial distribution of the beam was specified by a two-dimensional normal distribution with a width at half maximum in X and Y = 2 cm ($\sigma = 0.847 \text{ cm}$). The results of all calculations were normalized to 1 beam proton. The weight composition of concrete in the calculations was taken from [2]: H — 0.006276; C — 0.058996; O — 0.5159; Mg — 0.0041841; Al — 0.0075313; Si — 0.14728; S — 0.0037656; Ca — 0.251046; Fe — 0.0050209.

The geometry of the experiment simulated in the calculations is shown in Fig. 2. The spatial distribution (along the X-axis) of the yields of protons, neutrons, charged π -mesons, and gamma quanta from the shield, as well as the values of the absorbed dose (for all field components) at the site of animal irradiation (points 1–7), were calculated. The lower energy threshold for neutrons was taken equal to 10^{-9} MeV , for protons and π -mesons — 1 MeV, for gamma quanta — 0.1 MeV. The calculations were carried out with three shielding thicknesses of 20, 40, and 80 cm. The statistical accuracy of the calculations was better than 2% in the whole energy range.

Experimental verification of the secondary radiation fields validity

To check the validity of the calculations of the secondary radiation field behind the shields, carried out using the MCNPX program, the spatial distribution of the activation of aluminum detectors behind the shield 20 cm thick was measured. For the experiment, 7 detectors were prepared from chemically pure aluminum with dimensions of $2 \times 1.5 \text{ cm}$, weighing about 13.4 g. To measure gamma spectra from activated detectors, a scintillation gamma spectrometer based on NaI(Tl)

crystal with a diameter and height of 40 mm was assembled, connected to a PMT-93 photomultiplier.

A large radiochromic film was used to study the spatial distribution of ionizing radiation from a concrete wall at a point lying on the continuation of the trajectory of the primary proton beam.

At the central points of the assumed placement of the mice behind the concrete shields, the absorbed doses of radiation were measured with a diamond detector.

Results and discussions

Shield 20 cm

In Fig. 3–6 the calculated spectral distributions of the fluences of secondary particles and gammas averaged over volumes of 39.3 cm^3 ($\varnothing = 5 \text{ cm}$, $h = 2 \text{ cm}$) at points 1–7 behind the 20 cm shield are demonstrated. The ordinate shows the values of fluences in the energy bins (energy discretization interval). Neutron spectra are presented on a logarithmic scale from 10^{-8} to 10^3 MeV .

The ionization range of protons with an energy of 650 MeV in concrete is more than 20 cm. The spectra of secondary protons are formed mainly due to elastic and quasi-elastic scattering of primary protons on the shielding nuclei, but at point 4 in the center of the shield, the initial protons of the beam make an overwhelming contribution to the proton spectrum, partially lost their

energy in the thickness of the shield. The neutron spectra clearly show characteristic features associated with the accumulation of thermal neutrons (10^{-8} – 10^{-7} MeV), evaporative neutrons (1–10 MeV), and cascade neutrons (around 100 MeV). Behind thin shielding, the fraction of thermal neutrons is insignificant, because, firstly, there is very little chemically bound water in concrete, and secondly, neutrons in such a small layer of matter cannot thermalize. The threshold for π -meson production in nuclear reactions is about 300 MeV, so their energy also does not exceed 200–300 MeV. The maximums appear in the gamma-ray spectra correspond to the energies of annihilation gamma rays, and, probably, to the ~ 1.8 and $\sim 6 \text{ MeV}$ lines from silicon and oxygen. In the energy range $\sim 100 \text{ MeV}$, the accumulation of gamma rays is associated with the decay of π^0 -mesons, which are produced mainly in the direction of the primary proton beam.

The spatial distributions of the fluences of all components of the secondary radiation field behind the shield — neutrons, protons, π -mesons, and gamma rays, along the X-axis of a concrete shield 20 cm thick are shown in Fig. 7. The range of 650 MeV protons in concrete with a density of 2.15 g/cm^3 is 95.2 cm [5], i.e. formally exceeds the thickness of even the thickest shield 80 cm. Therefore, some of the primary beam protons that have not interactions in concrete escape from the shield at point 4, forming a sharp maximum in the spatial

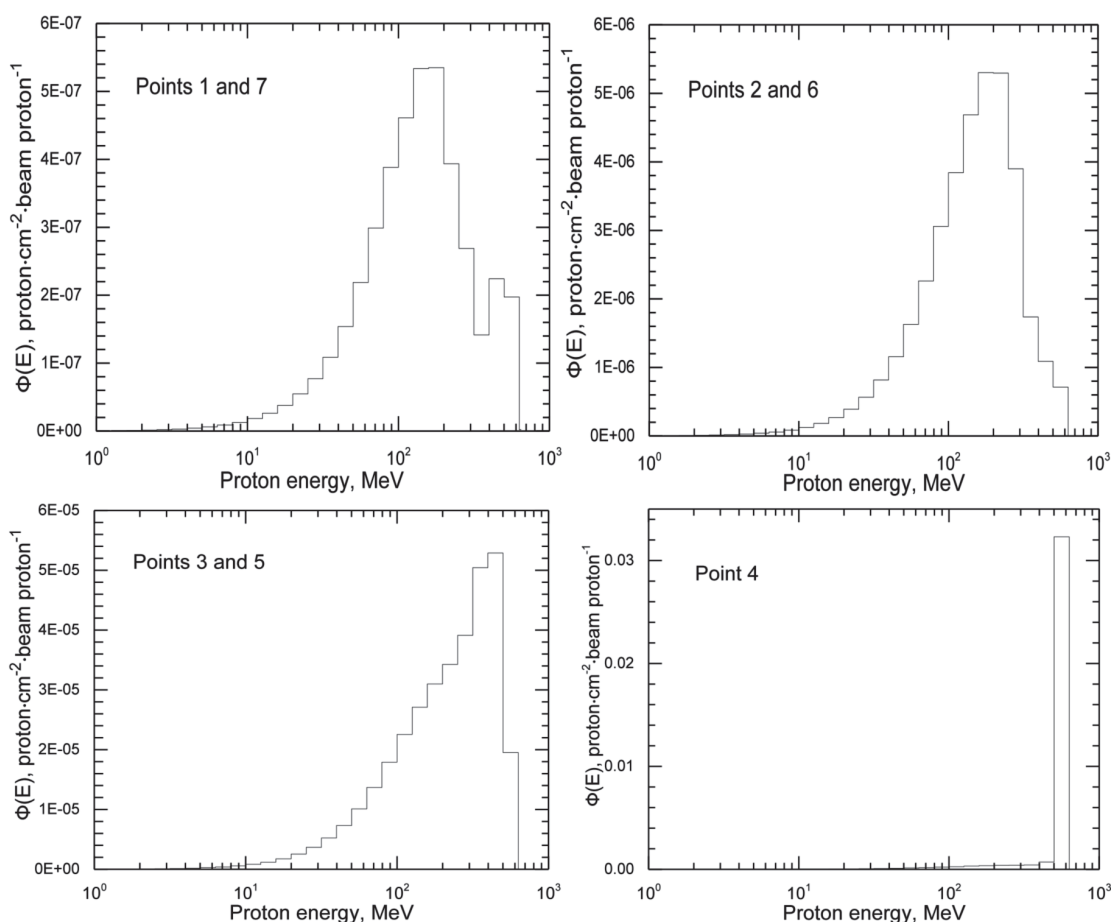


Fig. 3. Spectra of protons behind the 20 cm concrete shield

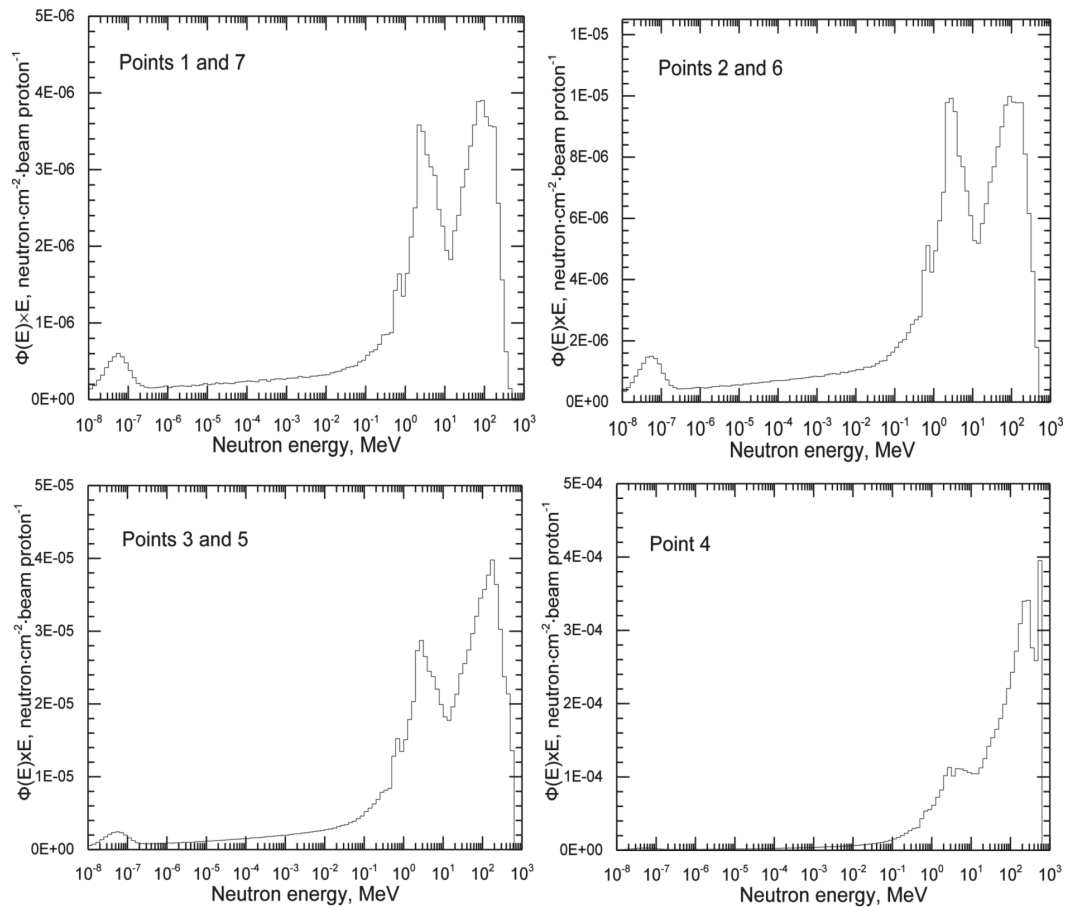


Fig. 4. Spectra of neutrons behind the 20 cm concrete shield

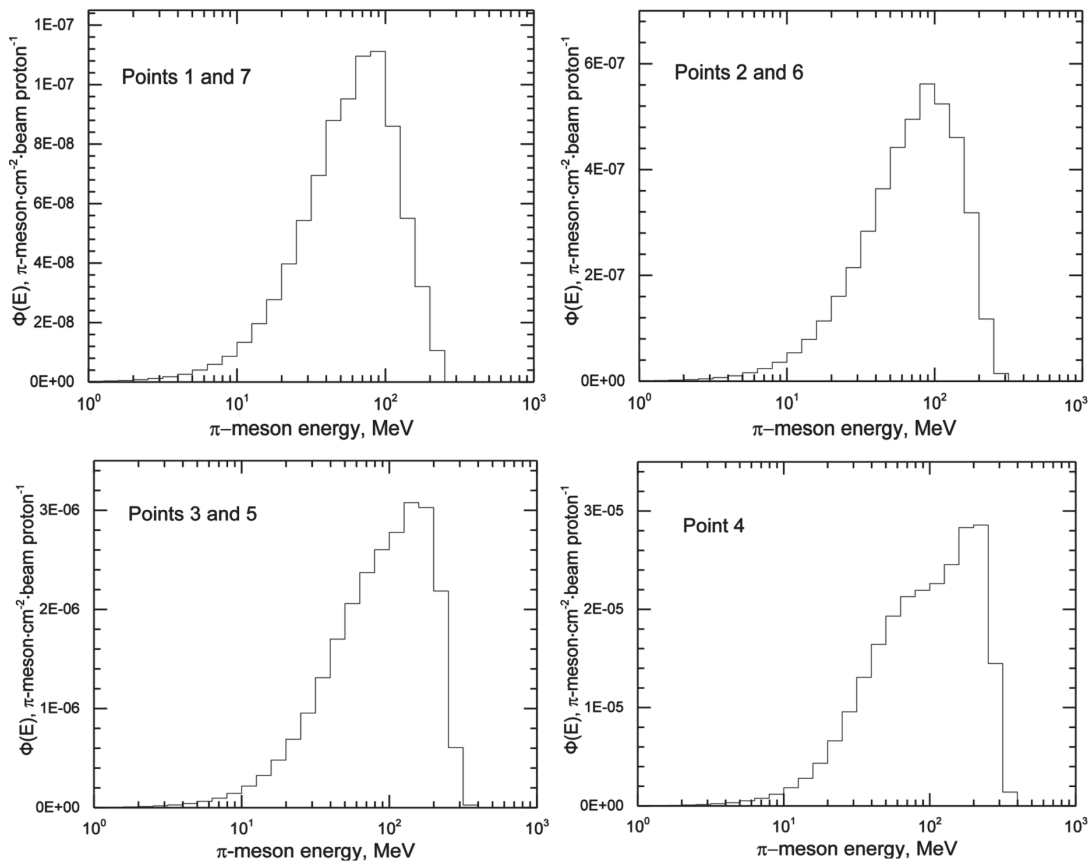


Fig. 5. Spectra of pi-mesons behind the 20 cm concrete shield

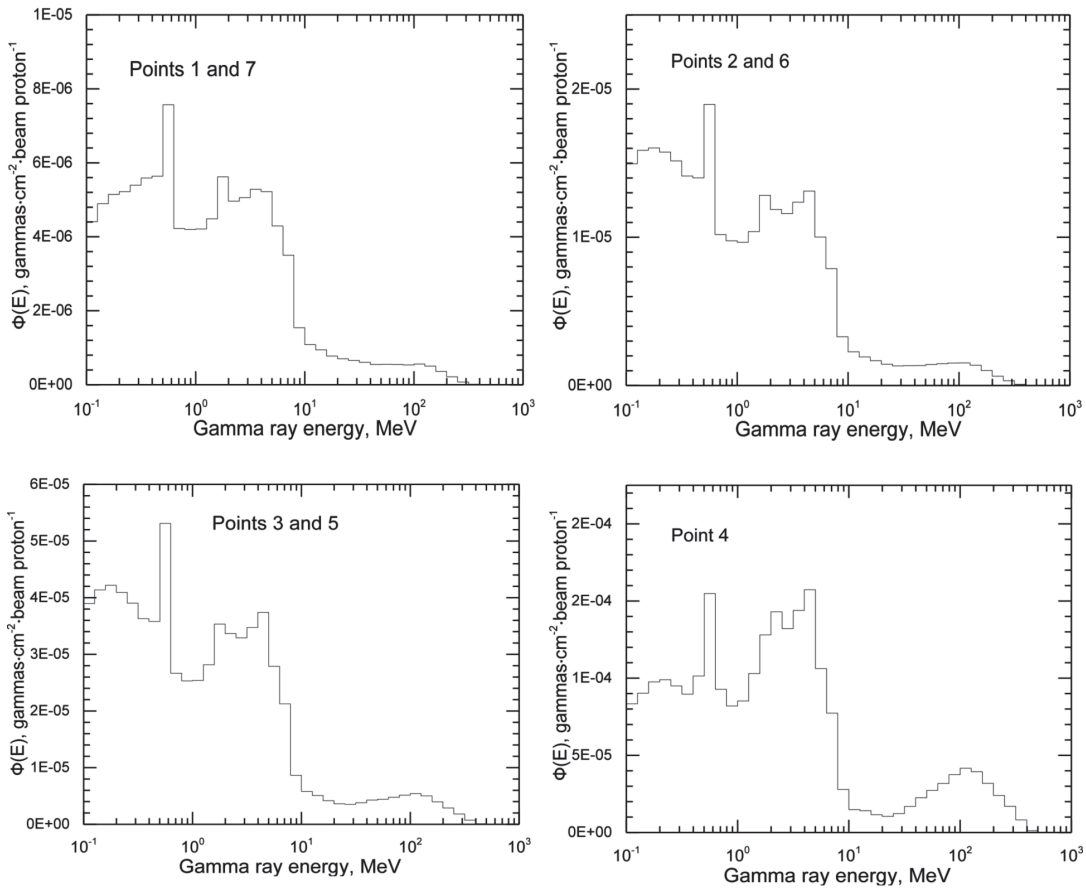


Fig. 6. Spectra of gamma rays behind the 20 cm concrete shield

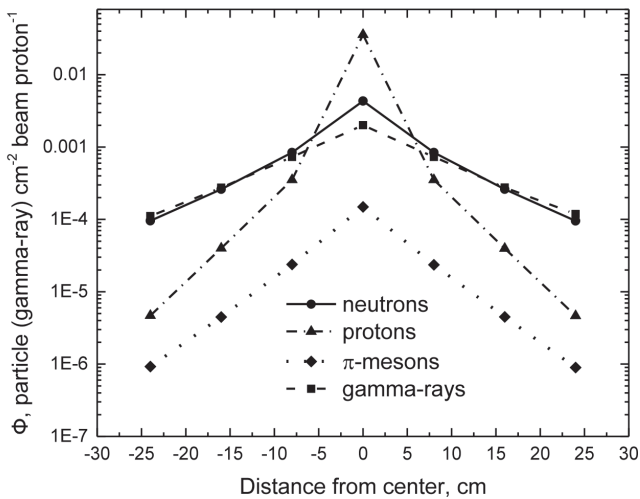


Fig. 7. Spatial distributions of neutrons, protons, π -mesons and gamma-rays behind the 20 cm concrete shield

distribution of the proton fluence. The spatial distribution of neutrons does not have a sharp maximum in the shield center, but on the edges of the shield, neutrons make an overwhelming contribution to the total hadron fluence. The production of gamma rays is mainly determined by the reactions of inelastic scattering or capture of neutrons, and the spatial distribution of gamma-ray

fluences practically coincides with the distribution of neutron fluences. Thus, the component composition of the radiation field behind the shield varies over a very wide range depending on the position of the point under consideration, since with such a thickness, concrete is more a multiplying target than a shielding. As a result, in the center of the shield, the main contribution to the dose will be created by high-energy protons, and at the edges of the shield, the dose will be created mainly by neutrons.

Shield 40 cm

In Fig. 8 the spatial distributions of the fluences of all components of the secondary radiation field along the X-axis of a 40 cm thick concrete shield are presented. The spatial distribution of hadron fluences behind the 40-cm shield is flatter than behind the 20-cm shield since, with an increase in the thickness of the shield, the internuclear cascade begins to play an increasing role, and protons at the edges of the shield are formed in the interactions of neutrons with nuclei in the last layer of the shield. The proton fluences in the central part of the shield are relatively reduced compared to the 20-cm shield, but the small-angle scattering of the primary beam protons, as well as some of the beam protons that have not any interactions with concrete, still create a sharp maximum of the field behind the shield along the beam axis. The number of π -mesons behind the shield also decreases due

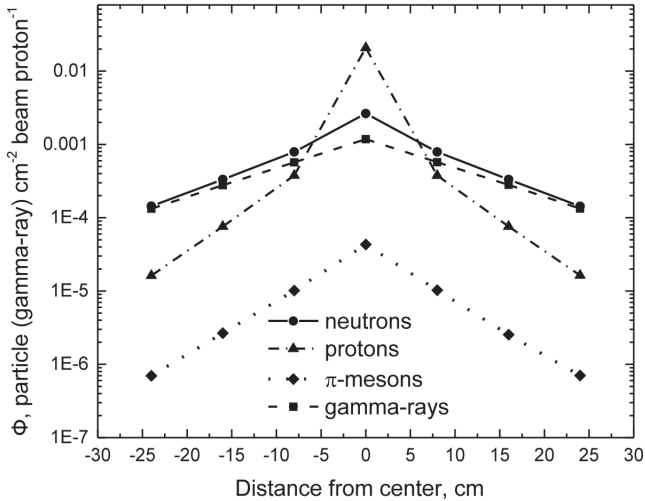


Fig. 8. Spatial distributions of neutrons, protons, π -mesons and gamma-rays behind the 40 cm concrete shield

to the lowering of the average energy of nucleons in the shield.

Shield 80 cm

The spatial distributions of the fluences of all components of the secondary radiation field along the X-axis behind the concrete shield 80 cm thickness are shown (Fig. 9). It's clear that behind the thick 80 cm shield, the spatial distributions of secondary hadrons are practically completely formed as a result of the internuclear cascade since the free path to inelastic interaction in the concrete of even high-energy neutrons (close to the energy of the primary protons of the beam) is about 40 cm. The yield of hadrons from the shield decreases because, with such shield thickness, radiation attenuation in concrete begins to prevail. Due to the dissipation of the nucleon's energy in the shield, the yield of π -mesons from it becomes negligible.

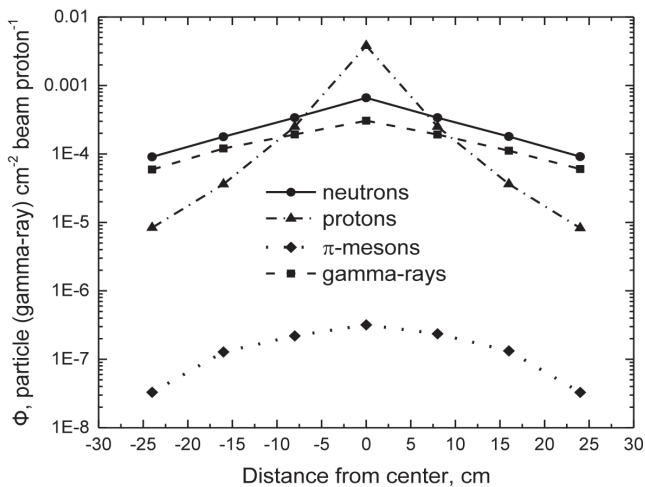


Fig. 9. Spatial distributions of neutrons, protons, π -mesons and gamma-rays behind the 80 cm concrete shield

In Fig. 10-11 the spectral distributions of the fluences of secondary nucleons at points 1, 7, and 4 behind the concrete shield 80 cm for comparison with the distributions behind the shield 20 cm thick are presented. In Fig. 10 it can be seen that at the central point behind the shield there is still a small fraction of the primary beam protons and protons generated in acts of small-angle elastic and quasi-elastic scattering. In general, the main part of protons is produced in neutron reactions in the last layer of the shield as a result of the internuclear cascade. Therefore, a large number of low-energy protons appear in the proton spectrum, in contrast to the proton spectra behind a 20 cm thick shield.

The neutron spectra in Fig. 11 are typical for neutron spectra behind thick shields. In the low-energy region, there is an accumulation of thermal neutrons, in the energy region of about 1 MeV there is an accumulation of evaporative neutrons, and in the region of ~ 200 MeV, there is a peak due to cascade neutrons. Comparison of the spectra of protons and neutrons behind shields 20 and 80 cm thick shows that the shielding thickness strongly affects the component and spectral composition of the secondary radiation field.

Experimental verification of the calculation of the secondary radiation field behind the concrete 20 cm shield

The verification of the calculations was carried out based on the threshold activation detectors at points 1-7 behind the shield 20 cm thick. In the experiment, the spatial distribution of the activation of aluminum detectors with the formation of ^{24}Na radionuclide was measured. A similar distribution of detector activity in saturation was calculated using the MCNPX code.

As a result of ^{27}Al activation (100 % abundance) by secondary protons, neutrons, and π -mesons, several radionuclides are formed (see Table 1), including the ^{24}Na radionuclide with a half-life of 14.96 hours, which emits two gamma lines with energies of 1.369 and 2.754 MeV (100 % yield per decay) [6].

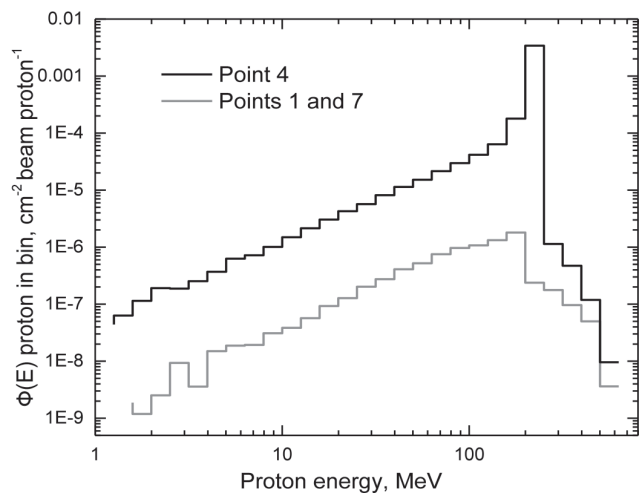


Fig. 10. Spectra of protons at points 1, 7 and 4 behind the shield 80 cm thick

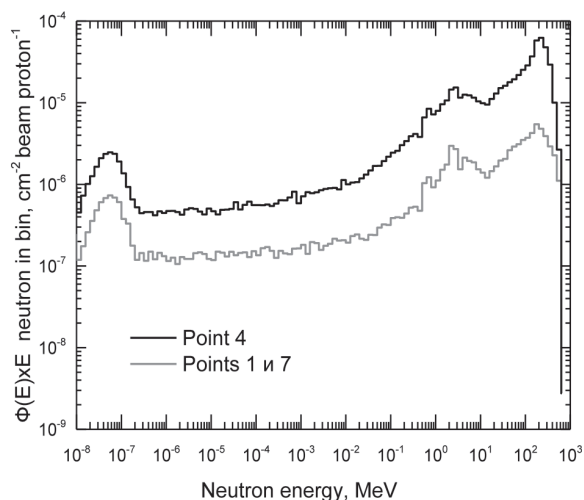


Fig. 11. Spectra of neutrons at points 1, 7 and 4 behind the shield 80 cm thick

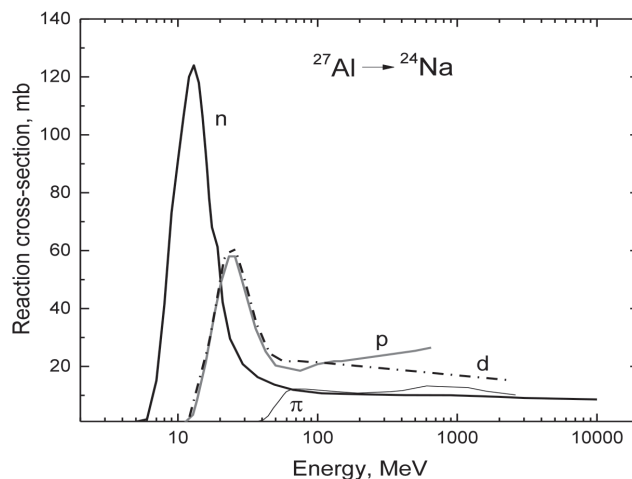


Fig. 12. Cross sections for the activation reactions of ²⁷Al by hadrons to form ²⁴Na

Table 1
Characteristics of radionuclides formed at the activation of ²⁷Al by high-energy hadrons

Radionuclides*	Reaction	Gamma line energy, MeV	Yield per decay, %	Half-life
²⁴ Na, β -decay	²⁷ Al(A, X) ²⁴ Na	3.8236 2.7541 1.3685	0.064 100 100	14.96 h
²² Na, β -decay	²⁷ Al(A, X) ²² Na	1.2745 0.511	100 180	2,602 y
²⁸ Al, β -decay	²⁷ Al(n, g) ²⁸ Al	1.779 0.511	100	2.24 min
²⁶ Al, β -decay	²⁷ Al(n, 2n) ²⁶ Al	1.809 0.55	100 164	720000 y
²⁷ Mg, β -decay	²⁷ Al(n, p) ²⁷ Mg	0.844 1.014	72 28	9.46 min
¹⁸ F, β -decay	²⁷ Al(A, X) ¹⁸ F	0.511	190	109.74 min
¹³ N, β -decay	²⁷ Al(A, X) ¹³ N	0.511	200	10 min
¹¹ C, β -decay	²⁷ Al(A, X) ¹¹ C	0.511	200	20.5 min
⁷ Be, e-capture	²⁷ Al(A, X) ⁷ Be	0.4776	10	53.44 d

Note: *The remaining possible radionuclides are either pure β -decayers or have very short half-lives (milliseconds and microseconds)

The half-lives of radionuclides ²²Na and ²⁶Al with energetic gamma lines and ⁷Be are much longer than the half-life of ²⁴Na, i.e. their activity is significantly lower than that of ²⁴Na. Radionuclides ²⁸Al, ²⁷Mg, ¹⁸F, ¹³N, and ¹¹C have half-lives much shorter than those of ²⁴Na, therefore, with appropriate delay after irradiation, their contribution to the total activity can also be made negligible. In fact, in the period from several hours to several tens of hours after the irradiation of a ²⁷Al detector, its induced activity is determined only by the ²⁴Na radionuclide. Another important practical advantage of ²⁴Na is the high energy of one of its lines — 2.754 MeV since there are practically no background events in this energy range when measuring the gamma spectrum from activated aluminum.

The cross-sections for the ²⁷Al activation reactions by neutrons, protons, and deuterons with the formation of ²⁴Na are shown in Fig. 12 [7]. There are no data on the similar activation of ²⁷Al by π -mesons.

For the experiment, we used activation detectors made of chemically pure aluminum. The measurement of gamma-ray spectra from activated detectors was carried out by a scintillation gamma-spectrometer based on a NaI(Tl) crystal with a diameter and height of 40 mm, placed inside a lead shield.

The activity of the detectors was measured 1 hour after irradiation, so that the short-lived nuclides ²⁸Al, ²⁷Mg, ¹³N, ¹¹C had time to decay. Corrections were made to the detector activity during the decay time between the end of irradiation and the beginning of spectra measurement on the spectrometer, as well as corrections for the detector irradiation time and measurement time. The measurement results were the saturation activities of the detectors due to the activation of ²⁷Al by the secondary radiation from the shield.

The comparison of the spatial distributions of activities in the saturation of aluminum detectors behind the 20 cm shield calculated using the MCNPX code and measured in the experiment is shown in Fig. 13. The calculation and experimental results are normalized to the readings of the central (4th) detector.

In general, the agreement between the calculation and experiment is quite satisfactory, taking into account the fact that the cross-section of the proton beam at the point of their entrance to the shield in the experiment (width at half maximum: in X — 5.3 cm, in Y — 4 cm) was noticeably wider than it was accepted in the calculation. This caused some expansion of the spatial distribution of hadron yields from the shield and, accordingly, the experimental spatial distribution of the detector activity in comparison with the calculation. The calculations also did not take into account the activation of detectors by π -mesons and background scattered radiation. The performed experimental verification gives reason to believe that the radiation fields behind the shields were

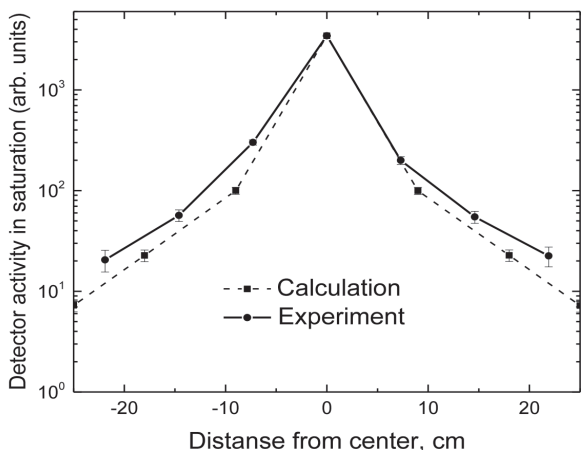


Fig. 13. Comparison of the calculated and measured spatial distributions of the activities of aluminum detectors behind the 20 cm thick shield

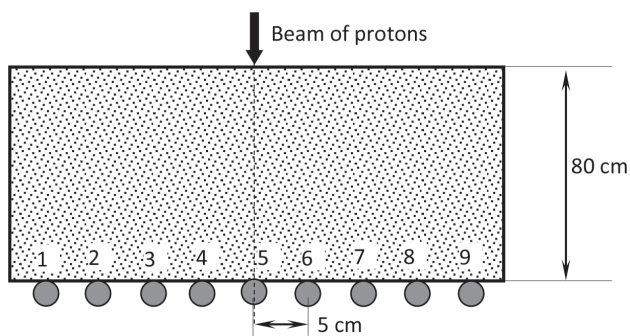


Fig. 14. Location of mouse phantoms behind the 80 cm thick shield

calculated using the MCNPX code with a high degree of reliability.

Calculation of absorbed doses in phantoms of mice behind concrete shields

The location of 9 phantoms of mice behind a concrete shield 80 cm thick is shown in Fig. 14. Mice were modeled with Ø 3.66 cm phantoms filled with water as an analog of biological tissue. The volume of the phantom corresponds to the weight of water 25 g — the average weight of an adult mouse.

For each phantom, the energy distributions of particles (protons, neutrons, charged π-mesons) and gamma rays averaged over the phantom volume were calculated, as well as the energy losses of radiation in its volume. Partial absorbed dose in the phantom volume for each radiation component was determined as a result of dividing the corresponding energy loss by the phantom mass. The calculated values of the absorbed doses in units of Gy/beam proton in mice phantoms from protons, neutrons, charged π-mesons, and gamma rays are given in Table 2.

Protons make an overwhelming contribution to the total absorbed dose of mice phantoms. The second most important component is neutrons, next is gamma rays and the least component is mesons.

Behind shields 40 and 20 cm thick, the values of the absorbed doses in the phantoms of mice were calculated in the extreme 1, 9, and the central phantom 5. The values of the absorbed doses, normalized to 1 beam proton, are given in Table 3.

Noteworthy is the fact that if for phantom 5 the dose decreases monotonically as the thickness of the shield increases, then for phantoms 1 and 9 (at the edges of the shield) the dose first increases at a thickness of 40 cm, and then begins to decrease (thickness of 80 cm). This is due to the mechanism of the secondary radiation field formation in the shielding. In extreme phantoms, the absorbed dose is mainly due to secondary neutrons. With an increase in

Table 2

Absorbed doses D per 1 beam proton in mice phantoms behind 80 cm shield

N° phantom	1	2	3	4	5	6	7	8	9
D neutrons, Gy	1.12E-14	1.65E-14	2.62E-14	4.11E-14	7.28E-14	4.61E-14	2.74E-14	1.70E-14	1.13E-14
D protons, Gy	2.04E-14	4.99E-14	1.33E-13	8.11E-13	3.29E-12	8.09E-13	1.38E-13	5.02E-14	1.94E-14
D gammas, Gy	6.52E-16	8.47E-16	1.19E-15	1.59E-15	1.97E-15	1.62E-15	1.17E-15	8.23E-16	5.71E-16
D π-mesons, Gy	3.46E-17	1.04E-16	1.13E-16	1.91E-16	2.08E-16	1.64E-16	1.19E-16	9.01E-17	5.05E-17
ΣD, Gy/beam proton	3.23E-14	6.73E-14	1.61E-13	8.60E-13	3.36E-12	8.57E-13	1.64E-13	6.81E-14	3.13E-14

Table 3

Absorbed doses D per 1 beam proton in mice phantoms behind 40 and 20 cm shields

Shield thickness	Shield 40 cm			Shield 20 cm			
	N° phantom	1	5	9	1	5	9
D neutrons, Gy		1.36E-14	3.29E-13	1.36E-14	9.44E-15	5.99E-13	9.44E-15
D protons, Gy		2.90E-14	1.94E-11	2.90E-14	1.50E-14	3.96E-11	1.50E-14
D π-mesons, Gy		8.26E-16	2.10E-14	8.26E-16	1.88E-15	7.46E-14	1.88E-15
D gamma rays, Gy		1.87E-15	1.40E-14	1.87E-15	2.14E-15	4.10E-14	2.14E-15
ΣD, Gy/beam proton		4.53E-14	1.97E-11	4.53E-14	2.97E-14	4.04E-11	2.97E-14

Table 4

Estimations of absorbed doses of mice in cells, Gy

N° cell	1	2	3	4	5	6	7	8	9
Shield 20 cm	0,11	0,27	0,73	4,52	13,9	6,8	0,55	0,33	0,23
Shield 40 cm	0,14	0,23	0,45	3,5	8,45	4,12	0,72	0,25	0,12
Shield 80 cm	0,11	0,21	0,5	1,6	2,65	1,1	0,21	0,17	0,1

the shield thickness, secondary neutrons first accumulate in it, and then the attenuation of their fluence according to the exponential law prevails. In phantom 5, in the center of the shield, the absorbed dose is determined by protons (including beam protons), the fluence of which behind the shield decreases with increasing shield thickness.

Comparison of the calculated absorbed doses behind shields with the results of dose measurements by diamond detectors

At the central points of the planned placement of the mice behind the concrete shields, the absorbed dose was measured with a diamond detector. This made it possible to compare, in the first approximation, the calculated and experimental values of the absorbed doses in the secondary field of mixed gamma-hadron radiation. Since the calculations were performed for one primary proton of the beam, the calculation data were normalized to the number of beam protons that bombarded the shield during the measurement with a diamond dosimeter for comparison with the experiment. Estimates showed that 3.73×10^{11} protons came to the shield during the measurements. The calculated values of absorbed doses in the central (5th) cell behind the shields were multiplied by this value with the experimental values of doses measured by a diamond detector. In all experiments, the proton dose at the entrance to the concrete shield was 25 Gy, with an average dose rate of 0.6 Gy/s.

Fig. 15 shows the results of comparing the calculations of absorbed doses in cells No. 5 behind the shields with the experimental values of doses measured by a diamond detector.

In whole, the agreement between the calculations and experiment is quite satisfactory, if we take into account the asymmetry of the proton beam profile that took place in some runs, caused by objective reasons (distortion of the left parts of the distribution behind the shields due to the conditions of formation of the primary proton beam, the presence of background gamma-rays and neutrons and differences in the absorbing medium in calculations and experiment (water phantom with a diameter of 3.66 cm and a diamond crystal with a volume of 5 mm³).

Then, the radiation doses were estimated at nine points of the proposed location of the mice (Fig. 14). The results are shown in Table 4. These estimations were

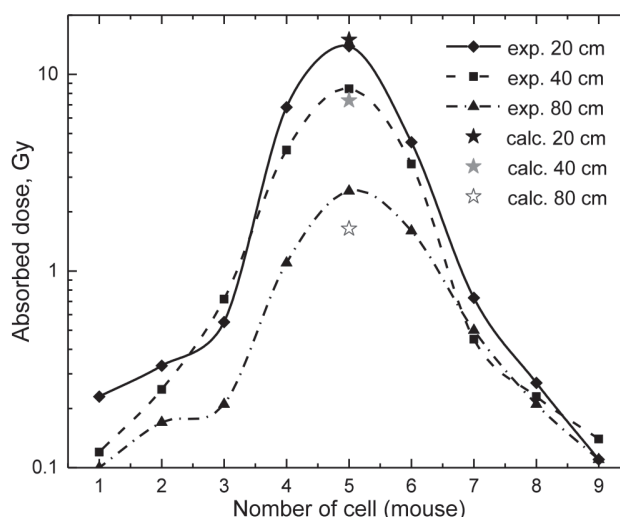


Fig. 15. Comparison of the calculated and experimental values of the absorbed dose behind shields with different thickness

carried out for carrying out a radiobiological experiment at this stand.

Conclusion

With a proton beam of the JINR phasotron the stand for radiobiological experiment behind concrete shields of various thicknesses was created. Calculations of the radiation fields generated in the shields have been carried out and, on their basis, the values of absorbed doses in the mice phantoms at several points behind the shields have been evaluated. Experimental checks of the calculations in the points of the mice placement were carried out using activation detectors and a diamond detector. Radiobiological experiments on animals at this stand are planned in the interests of designing a protective building on the Moon and other space bodies, as well as at charged particle accelerators.

Acknowledgment

The authors thank the head of the laboratory of the State Research Center – A.I. Burnasyan Federal Medical Biophysical Center of Federal Medical Biological Agency Igor Nikolaevich Sheino for valuable recommendations on the presentation of these experiments in the article.

Моделирование условий облучения лабораторных животных за локальной бетонной защитой, облучаемой протонами с энергией 650 МэВ

А.А. Иванов^{1,2,3}, А.Р. Крылов¹, А.Г. Молоканов¹, А.Ю. Бушманов², А.С. Самойлов²,
Е.Е. Павлик¹, Г.В. Мицин¹, С.В. Швидкий¹, Г.Н. Тимошенко^{1,4}

¹ Объединенный институт ядерных исследований, Дубна

² Федеральный медицинский биофизический центр им. А.И. Бурназяна ФМБА России, Москва

³ Институт медико-биологических проблем РАН, Москва,

⁴ Государственный университет “Дубна”, Дубна

E-mail: tim@jinr.ru

РЕФЕРАТ

Приведены результаты расчета характеристик поля смешанного вторичного излучения за локальными бетонными защитами толщиной 20, 40 и 80 см, облучаемых пучком протонов с энергией 650 МэВ на фазотроне ОИЯИ, а также оценки значений поглощенной дозы облучения лабораторных животных за защитами в ходе радиобиологического эксперимента. Расчет выполнен методом Монте-Карло по программе MCNPX для вторичных протонов, нейтронов, пи-мезонов и гамма-квантов. С целью проверки достоверности расчетов было выполнено сравнение расчетных и измеренных в эксперименте пространственных распределений активации пороговых алюминиевых детекторов за защитами. Сравнение показало хорошее согласие между экспериментальными и расчетными величинами.

Ключевые слова: пучок протонов, поле вторичного излучения, поглощенная доза, транспорт излучений в веществе, бетонная защита, радиобиологический эксперимент

Для цитирования: Иванов А.А., Крылов А.Р., Молоканов А.Г., Бушманов А.Ю., Самойлов А.С., Павлик Е.Е., Мицин Г.В., Швидкий С.В., Тимошенко Г.Н. Моделирование условий облучения лабораторных животных за локальной бетонной защитой, облучаемой протонами с энергией 650 МэВ. Медицинская радиология и радиационная безопасность. 2020;65(5):77-86.

DOI: 10.12737/1024-6177-2020-65-5-77-86

СПИСОК ЛИТЕРАТУРЫ / REFERENCES

1. Ignatova AM, Ignatov MN. Use of resources for regolith exploration of the lunar surface. Int J Exper Education. 2013;11:101-10. (In Russ.).
2. Broder DL, Zaitsev LN, Komochkov MM. Concrete in the protection of nuclear installations. Atomizdat, Moscow. 1966. (In Russ.).
3. MCNPX User's Manual Version 2.6.0, April 2008 LA-CP-07-1473

4. Ivanov AA, Molokanov AG, Shurshakov VA, et al. Modification of the proton team physical parameters and radiobiological characteristics by elements of spacecraft radiation protection. Aerospace and Environmental Medicine. 2015;49(5):36-42. (In Russ.).
5. <http://www.nea.fr/abs/html/nea-0919.html>.
6. Reference Neutron Activation Library. IAEA-TECDOC-1285. Vienna. 2002.
7. <http://www-nds.iaea.org/exfor>.

Конфликт интересов. Авторы заявляют об отсутствии конфликта интересов.

Conflict of interest. The authors declare no conflict of interest.

Финансирование. Исследование не имело спонсорской поддержки.

Financing. The study had no sponsorship.

Участие авторов. Статья подготовлена с равным участием авторов.

Contribution. Article was prepared with equal participation of the authors.

Поступила: 19.10.2020. **Принята к публикации:** 11.11.2020.

Article received: 19.10.2020. **Accepted for publication:** 11.11.2020.

Information about the authors:

Ivanov A.A. <https://orcid.org/0000-0001-8403-8636>.

Timoshenko G.N. <https://orcid.org/0000-0001-8801-5319>.